Supplementary information:

Insight into the structure of black coatings of ancient Egyptian mummies by advanced Electron magnetic resonance of vanadyl complexes.

Charles E. Dutoit,[1] Laurent Binet,[1] Hervé Vezin,[2] Océane Anduze,[1] Agnès Lattuati-Derieux,[3] Didier Gourier [1]

[1] Chimie-ParisTech, PSL University, CNRS, Institut de Recherche de Chimie-Paris (IRCP), F-75005 Paris, France

[3] Centre de Recherche et de Restauration des Musées de France (C2RMF), Palais du Louvre, F-75001 Paris, France

[2] Université de Lille, CNRS, UMR8516-LASIRE, F-59000 Lille, France.

Correspondence to : Didier Gourier (didier.gourier@chimieparistech.psl.eu)

Table of content :

S1 Samples

Table S1. Description of samples

Samples	Object	Provenance	Origin /Dating	Description
Ref 1	Natural asphalt	C2RMF	Dead Sea, floating blocks (Late Cretaceous)	Black solid
Ref 2	Bitumen of Judea	C2RMF	Commercial	Brown powder
Hum 1	Anthropomorphic coffin	The Art and History museum of Narbonne, France (Ref: C2RMF76267)	Upper Egypt (Abydos ?). Ptolemaïc period (332 BC – 30 BC)	Coffin of Irethorerou, servant of Khonsou, of the White Crown and of Horus. Black matter covering the bottom of the coffin
Hum 2	Human mummy	The Hieron museum, Paray-le-Monial, France (Ref: FZ30827)	Late Period, end of the IVth century BC	Mummy of a 35-45 years old man, named …djeb. Set of crossed bands, coated with dark matter
Hum 3	Human mummy	Museum of Boulogne, France (Ref. 35906)	Late period, XXVth dynasty (744 BC - 656 BC)	Mummy found in the coffin of Nehemsimontou, coated with black matter.
An 1	Ram mummy	The Louvre museum, Paris, France; (Ref: C2RMF 64621)	Upper Egypt (Elephantine). Late period (672 BC–322 BC)	Fragment of black matter covering the mummy
An 2	Ram mummy	The Thomas Dobrée museum, Nantes, France (Ref: C2RMF36230)	Upper Egypt. Late Period (664 BC – 332 BC).	Fragments of black matter covering the mummy.
An 3	Ram mummy (the same as **An 2**)	The Thomas Dobrée museum, Nantes, France (Ref: C2RMF36230)	Upper Egypt. Late Period (664 BC – 332 BC).	fragments of tissue strips covering the mummy, coated with a brown material
An 4	Crocodile mummy	Musée des confluences, Lyon, France (Ref : 90001841)	Upper Egypt (Kom Ombo). Ptolemaïc period	Posterior part of mummified crocodile skull, covered with black matter.

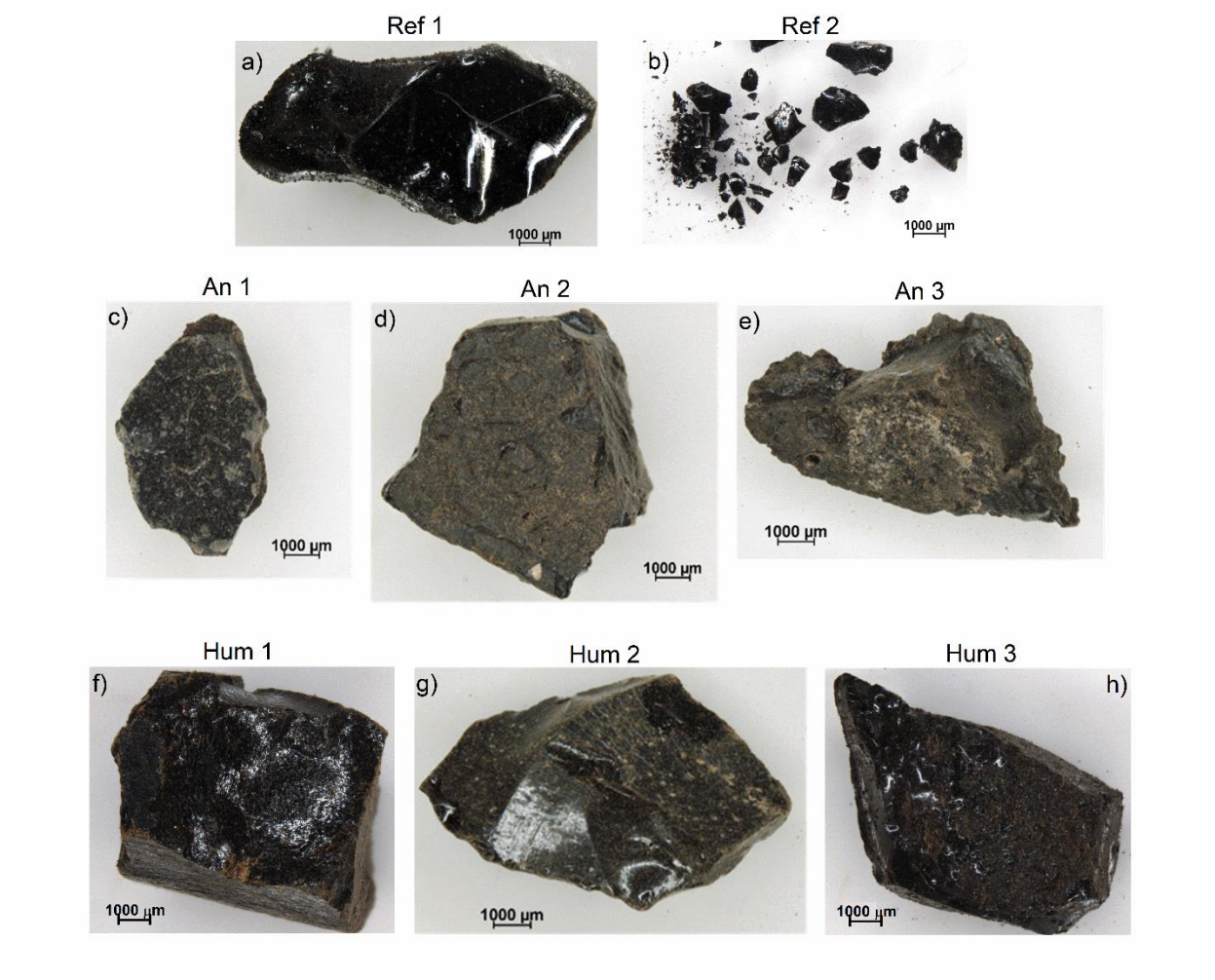

Figure S1. Binocular photographs of the samples studied in this work. © C2RMF.

S2 EPR spectra:

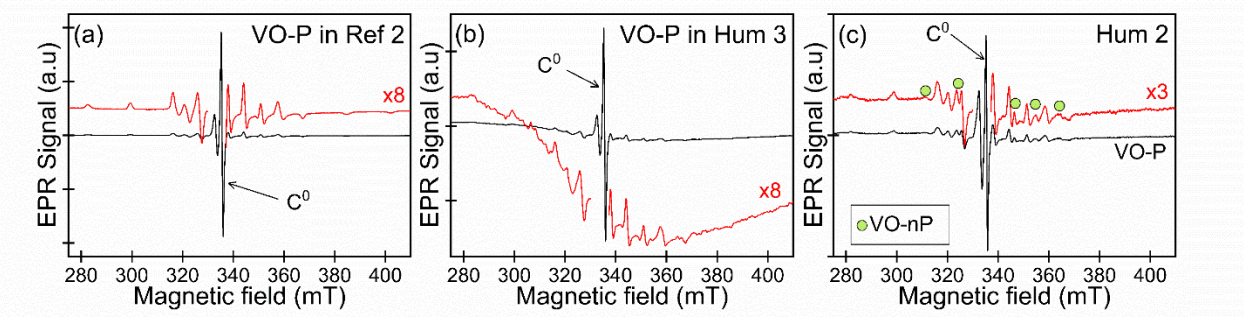

Figure S2. EPR spectra at X band and at room temperature of bitumen reference and human mummies: (a) ***Ref 2***, (b) ***Hum 3*** and (c) ***Hum 2***. This highlights the lack of VO-nP complexes (green circles) in ***Ref 2*** and ***Hum 3***.(From Dutoit, et al., 2020)

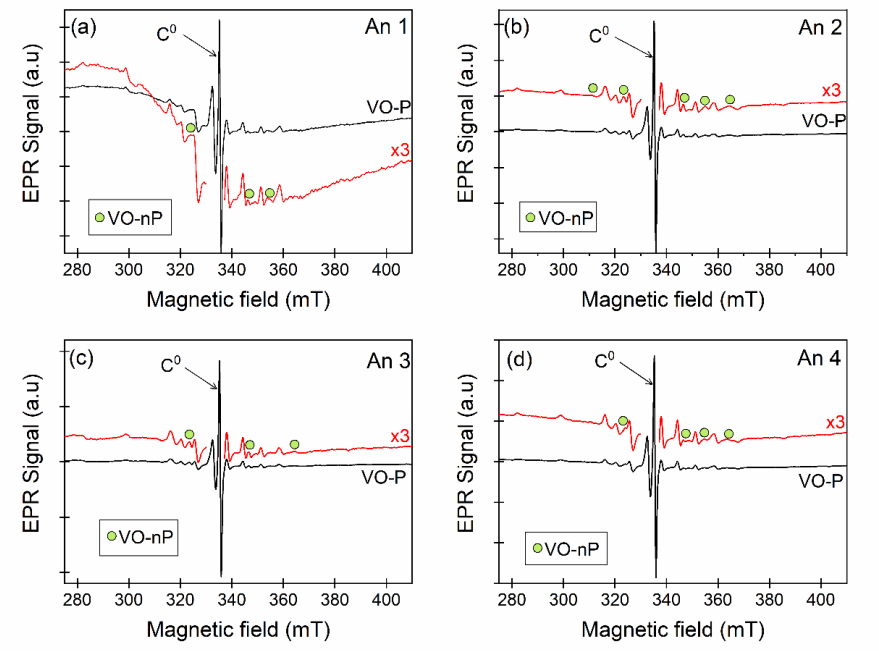

Figure S3. EPR spectra at X band and at room temperature of animal mummies, highlighting EPR lines of VO-nP complexes in (green circles). (From Dutoit, et al., 2020)

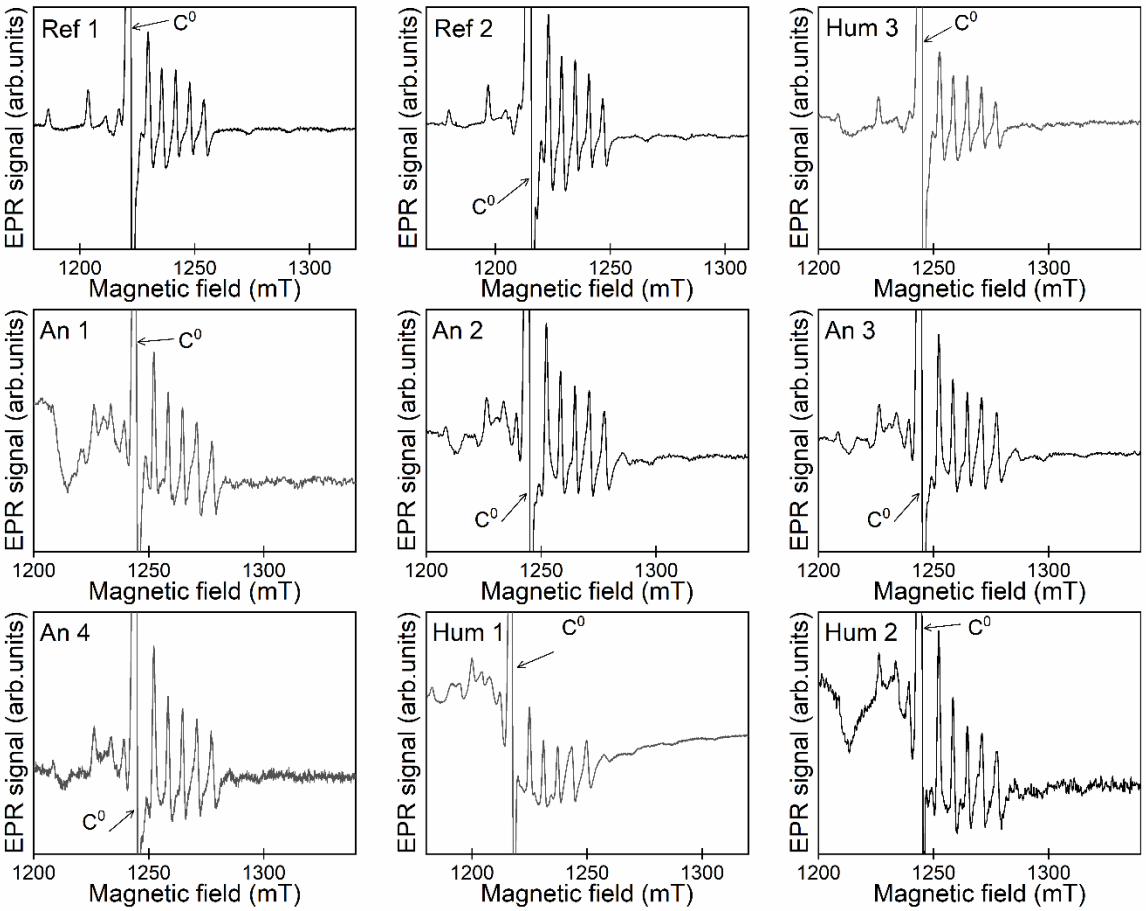

Figure S4. EPR spectra at Q band and at 100 K of the reference bitumen and samples of black coatings.

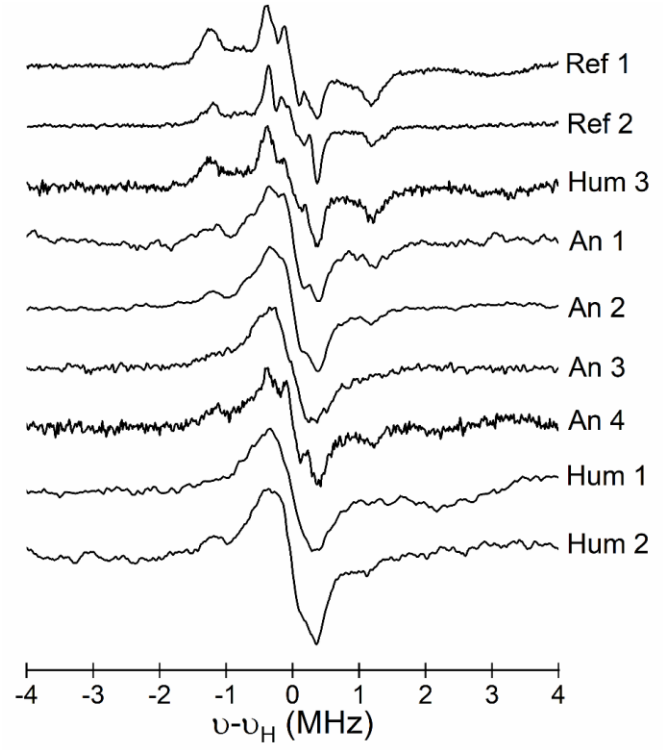

Figure S5. ^{1}H ENDOR spectra at Q band and at 100K of the reference bitumen and samples of black coatings.

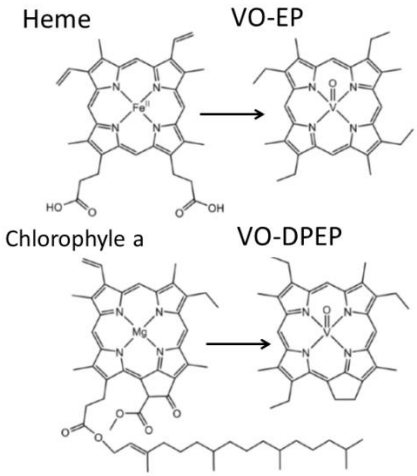

Figure S6. Two examples of geoporphyrins commonly found in oil, with the corresponding parent biomolecules

S4 Derivation of Equation 1

The ^{1}H ENDOR spectrum is the superposition of two independent signals: (i) one from the protons of the C-H$_{meso}$ bridges linking pyrole groups of porphyrin ligands, hereafeter referred to as VOP-^{1}H, and (ii) the other one from the matrix protons, hereafeter referred to as M-^{1}H, corresponding to protons of asphaltene, of the natural substances of the black matter, and of protons of alkyl substituent in porphyrin ligands. M-^{1}H protons are characterized by a pure dipolar hf interaction while VOP-^{1}H protons are characterized by an isotropic hf interaction in addition to the dipolar one.

Let X be the signal height at the frequency $\nu_{\parallel}$ corresponding to the parallel component of the VOP-^{1}H signal and Y the signal height at the maximum of perpendicular component of the VOP-^{1}H at frequency $\nu_{\perp}$ (see Fig.4a). Let also X_{VOP}, X_M, Y_{VOP} and Y_M be the respective contributions of a *single* VOP molecule and a *single* M-^{1}H to X and Y. Then :

$$\frac{X}{Y} = \frac{N_{VOP}X_{VOP} + N_M X_M}{N_{VOP}Y_{VOP} + N_M Y_M} \qquad \text{(S1)}$$

where N_{VOP} and N_M are the total numbers of VOP molecules and matrix protons in the sample, respectively.

The VOP molecules are embedded in bitumen aggregates spread within a bioorganic matrix, which contains the M-^{1}H's. As the M-^{1}H's are detected upon saturating an EPR transition of the VOP molecules, they must have a residual dipolar hf interaction with the VOP's. We thus assume that the detected M-^{1}H's are in a layer of volume V_L surrounding a bitumen aggregate (Fig. S7), then $N_M = N_A V_L [H]$ where N_A is the total number of bitumen aggregate in the sample and $[H]$ the concentration of M-^{1}H's in the matrix. We also have $N_{VOP} = [VOP]V$, with $[VOP]$ the concentration of VOP's in the sample and V, the sample volume. As the experimental variable is $x = [VOP]/[VOP]_{ref}$, where $[VOP]_{ref}$ is the VOP concentration in the reference sample ***Ref 1***, N_{VOP} is then rewritten as $N_{VOP} = x[VOP]_{ref}V$, yielding: $\frac{N_M}{N_{VOP}} = \frac{a}{x}$, with $a = N_A \frac{V_L}{V} \frac{[H]}{[VOP]_{ref}}$. Finally, we obtain:

$$\frac{X}{Y} = \frac{X_{VOP}}{Y_{VOP}} \times \frac{x + aX_M / X_{VOP}}{x + aY_M / Y_{VOP}} \qquad \text{(S2)}$$

From the ENDOR spectrum of ***Ref 1*** dominantly made of the contribution of VOP-^{1}H signal and negligible contribution from M-^{1}H, we get $\frac{X_{VOP}}{Y_{VOP}} \approx 0.625$ and assuming a gaussian lineshape for the M-^{1}H ENDOR line, we get $\frac{X_M}{Y_M} \approx 0.03$ giving $\frac{X_M}{X_{VOP}} \approx 0.048 \frac{Y_M}{Y_{VOP}}$ and finally:

$$\frac{X}{Y} \approx 0.625 \times \frac{x + 0.048 \times b}{x + b} \qquad \text{(S3)}$$

with a single adjustable parameter $b = a\frac{Y_M}{Y_{VOP}}$, which depends on the sizes and dispersion of the bitumen aggregates through N_A and the ratio $\frac{V_L}{V}$.

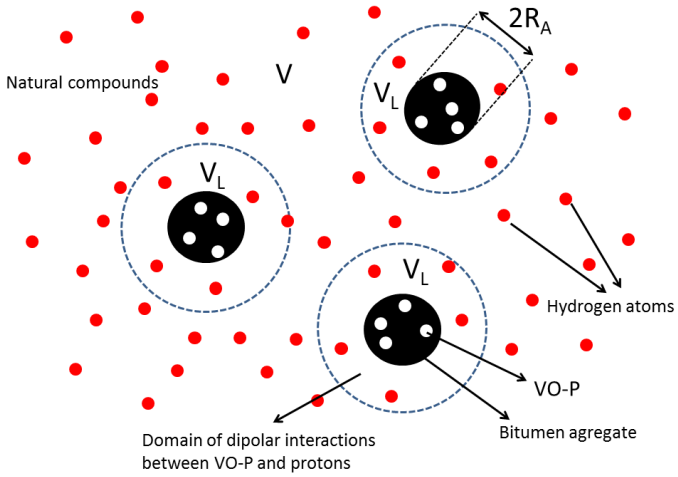

Figure S7. Schematic description of a bitumen aggregate in interaction with protons of bioorganic compounds.

S5 HYSCORE spectra of *Ref 2*

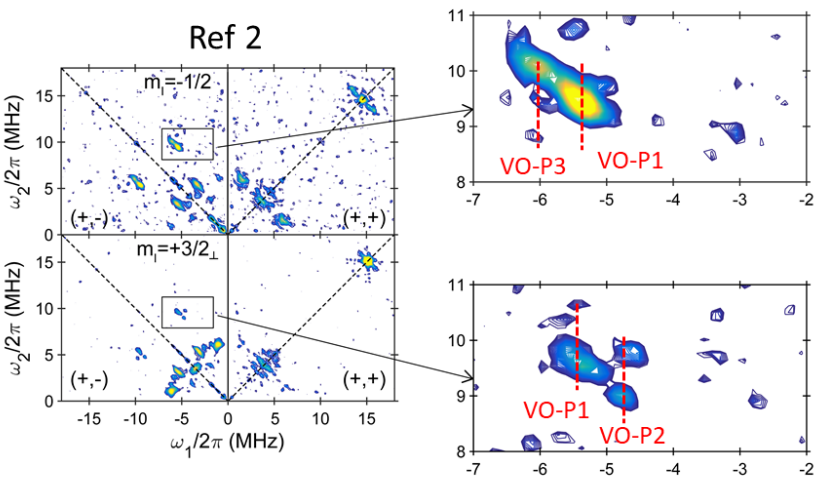

Figure S8. HYSCORE spectra of ***Ref 2*** recorded by observing the two EPR transitions m_I = -1/2 and m_I = +3/2⊥. Figures on the right show the portions of spectra corresponding to the frequency range of dq-dq correlations. Correlations sq-dq are not clearly detected because the VO-P content is lower in ***Ref 2*** than in ***Ref 1***.

S6 Estimation of second order contributions in ^{14}N parameters from dq-dq and sq-dq correlation peaks

The first order nuclear spin energy levels of a single m_s state of VO^{2+} interacting with the nuclear spin $I = 1$ of a ^{14}N nucleus is given by:

$$E = \pm\frac{1}{2}Am_I + Q\left(\frac{3}{2}m_I^2 - 1\right) - \nu_N m_I \qquad \text{(S4)}$$

where the energy E, the hf interaction A and the quadrupolar interaction Q are taken along the direction of the magnetic field. The corresponding energy level diagram is given in Fig. S9 for the two m_s states. The frequencies of the single quantum ($\Delta m_I = \pm 1$) and double quantum ($\Delta m_I = \pm 2$) nuclear spin transitions of ^{14}N are given by (Reijerse, et al., 1998; Dikanov, et al., 2004):

$$\nu_{1sq}^{\pm} = \frac{A}{2} \pm \nu_N + \frac{3Q}{2} + (2^{\text{nd}}\ \text{order terms})$$
$$\nu_{2sq}^{\pm} = \frac{A}{2} \pm \nu_N - \frac{3Q}{2} + (2^{\text{nd}}\ \text{order terms}) \qquad \text{(S5)}$$

$$\nu_{dq}^{\pm} = A \pm 2\nu_N + \frac{A^{(2)}}{(A/2) \pm \nu_N} \qquad \text{(S6)}$$

The second order corrections $\nu^{(2)}$ to the single quantum frequencies $\nu_{1sq}^{\pm}$ and $\nu_{2sq}^{\pm}$ are:

$$\begin{aligned}\nu_{1,2\mathrm{sq}}^{(2)+} &= \left(A^{(2)} \pm Q^{(2)}\right) \Big/ \left(A - 2\nu_N\right) \\ \nu_{1,2\mathrm{sq}}^{(2)-} &= \left(A^{(2)} \pm Q^{(2)}\right) \Big/ \left(A + 2\nu_N\right)\end{aligned} \qquad \text{(S7)}$$

where

$$\begin{aligned}A^{(2)} &= 1/4\left(T_{np}^2 + T_{nq}^2\right) + K^2\left(3 + \eta^2\right) - 3Q_n^2/4 \\ Q^{(2)} &= 3\left(Q_{np}T_{np} + Q_{nq}T_{nq}\right)\end{aligned} \qquad \text{(S8)}$$

$K = e^2qQ/4h$ is the quadrupolar coupling constant. The matrix elements T_{np} and T_{nq} in $A^{(2)}$ and $Q^{(2)}$ are anisotropic components of the hf interaction, **n** is the orientation of the magnetic field, and **p** and **q** are two orientations perpendicular to **n** and to each other.

Determination of *A* from expressions of $\nu_{dq}^{\pm}$ is not affected by 2nd order correction:

$$A = \frac{2\nu_N\left(\nu_{dq}^{+} + \nu_{dq}^{-}\right)}{8\nu_N - \left(\nu_{dq}^{+} - \nu_{dq}^{-}\right)} \qquad \text{(S9)}$$

On the contrary, measurement of *Q* from expressions from Eqs.S5 is affected by second order corrections and necessitates the preliminary determination of $\nu_{1sq}^{\pm}$ and $\nu_{2sq}^{\pm}$. As only a part of the sq-dq correlations has been detected, only half of then sq frequencies could be determined precisely. The observed sq-dq correlations for VO-P1 and VO-P2 correlate the dq transition of the m_s = +1/2 state with one of the sq transitions of the m_s = -1/2 state, and recalling that $\nu_{1sq}^{-} + \nu_{2sq}^{-} = \nu_{dq}^{-}$, all transitions in the m_s = -1/2 state are known without uncertainty due to 2nd order corrections. Single-quantum transitions in the m_s =+1/2 state were obtained to 1st order by the equation $\nu_{1sq}^{+} - \nu_{1sq}^{-} \approx \nu_{2sq}^{+} - \nu_{2sq}^{-} \approx 2\nu_N$ and are thus affected by 2nd order corrections. The resulting diagrams for VO-P complexes are given in Fig.S9. In the absence of unambiguous sq-dq correlations for VO-P3 and VO-P4, we could not obtain sq frequencies and quadrupolar parameter *Q* for these complexes.

The second order term in Eqs. S5, S6, S7 and S8 can be estimated as follows. Combining the two dq frequencies gives:

$$\nu_{dq}^{+} - \nu_{dq}^{-} = 4\nu_N - \frac{2\nu_{\mathrm{n}}\mathrm{A}^{(2)}}{A^2/4 - \nu_N^2} \qquad \text{(S10)}$$

From the experimental values of $\nu_{dq}^{\pm}$ and from ν_N = 1.1 MHz, we obtain $\mathrm{A}^{(2)}$ = 0.55 MHz and 0.44 MHz in VO-P1 and VO-P2, respectively. This gives a second order contribution $\frac{\mathrm{A}^{(2)}}{(A/2) \pm \nu_N} \approx 0.1 - 0.2$ MHz in Eq. S6 for VO-P complexes, which corresponds also to the uncertainty in the experimental measurement of dq frequencies in Fig. 6.

Concerning second order contributions in the determination of the quadrupolar interaction Q, expressions for sq frequencies give $\nu_{1sq}^{+} - \nu_{2sq}^{+} = 3Q + \frac{Q^{(2)}}{A/2 + \nu_N}$ and $\nu_{1sq}^{-} - \nu_{2sq}^{-} = 3Q + \frac{Q^{(2)}}{A/2 - \nu_N}$, which gives an estimation $Q^{(2)} \approx 0.5$ MHz of the same order as $A^{(2)}$, and thus $\frac{Q^{(2)}}{A/2 \pm \nu_N} \approx 0.1 - 0.2$ MHz.

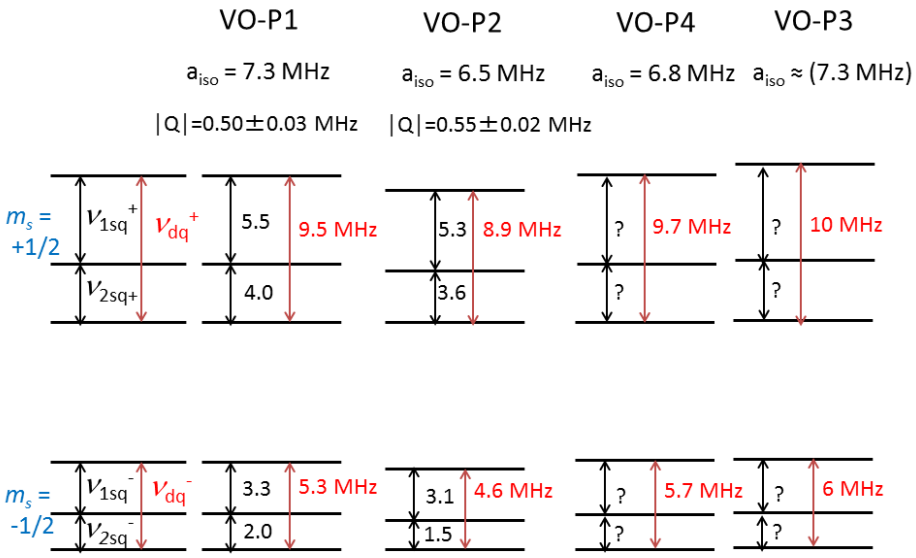

Figure S9. Energy level diagram of an electron spin $S = 1/2$ interacting with a nuclear spin $I = 1$, showing single quantum (sq) transitions (in black) and double quantum (dq) transitions (in red), with the corresponding diagrams for the four VO-Ps detected in the black matter; the four experimental diagrams correspond to the observation of the EPR transition $m_I = +3/2_{\perp}$ (for VO-P1, VO-P2 and VO-P4) and $m_I = -1/2$ for VO-P3; the quadrupolar interaction can be measured from sq transitions only when sq-dq peaks are detectable (VO-P1 and VO-P2); a_{iso} was deduced from dq-dq transitions obtained with the two EPR transitions $m_I = -1/2$ and $m_I = +3/2_{\perp}$.